Biofilms

Deutsche Ausgabe: DOI: 10.1002/ange.201605296
Internationale Ausgabe: DOI: 10.1002/anie.201605296

A Multinuclear Metal Complex Based DNase-Mimetic Artificial Enzyme: Matrix Cleavage for Combating Bacterial Biofilms

*Zhaowei Chen[+], Haiwei Ji[+], Chaoqun Liu, Wei Bing, Zhenzhen Wang, and Xiaogang Qu**

Abstract: *Extracellular DNA (eDNA) is an essential structural component during biofilm formation, including initial bacterial adhesion, subsequent development, and final maturation. Herein, the construction of a DNase-mimetic artificial enzyme (DMAE) for anti-biofilm applications is described. By confining passivated gold nanoparticles with multiple cerium(IV) complexes on the surface of colloidal magnetic Fe_3O_4/SiO_2 core/shell particles, a robust and recoverable artificial enzyme with DNase-like activity was obtained, which exhibited high cleavage ability towards both model substrates and eDNA. Compared to the high environmental sensitivity of natural DNase in anti-biofilm applications, DMAE exhibited a much better operational stability and easier recoverability. When DMAE was coated on substratum surfaces, biofilm formation was inhibited for prolonged periods of time, and the DMAE excelled in the dispersion of established biofilms of various ages. Finally, the presence of DMAE remarkably potentiated the efficiency of traditional antibiotics to kill biofilm-encased bacteria and eradiate biofilms.*

Bacteria in natural, clinical, and industrial settings tend to attach to surfaces and organize themselves into multicellular communities known as biofilms. In biofilms, microbes are held together by self-synthesized extracellular polymeric substances (EPS), which are typically composed of polysaccharides, proteins, and extracellular DNA (eDNA).[1] Shielded within such sticky and strong frameworks, biofilm-enclosed bacteria are markedly more resistant to antibiotics, host immune defenses, and environmental stresses than planktonic ones.[2] In turn, the inability to completely eliminate bacterial biofilms, particularly those formed on tissues or medical devices, often leads to persistent infections, implant failure, and even death.[3] Furthermore, biofilms are highly damaging towards industrial devices, clogging filtration membranes, fouling marine surfaces, and corroding pipes, for example.[4] As a result, combating bacterial communities has remained a prime challenge for decades.

Recently gained insight into the molecular mechanisms behind biofilm formation provides useful information for the development of new approaches for biofilm destruction.[5] Specially, as the longest molecule in EPS, eDNA acts as a bridge to enhance the initial bacterial surface adhesion and subsequent cellular aggregation as well as to connect bacteria with other EPS components to form mature networks, ultimately keeping all constituents together.[6] The process mainly involves attractive acid–base interactions, Lifshitz/van der Waals forces, and specific or non-specific mechanisms.[6] The cleavage of this pivotal EPS component by DNase has been proposed to prevent biofilm formation, disintegrate preformed biofilms, and sensitize the encased bacteria to antibiotics.[7] Nevertheless, to prevent biofilm formation, continued addition of DNase to new generations of bacteria is required owing to the lack of long-term activity and difficulty in recovery, which leads to high costs.[7] Furthermore, when trying to disperse established biofilms, the retarded permeation into and diffusion within biofilms and digestion by proteolytic exoenzymes largely impact the activity of subsequently added DNase, as there are issues with the high environmental sensitivity and low operational stability of natural enzymes.[7] These drawbacks greatly limit the practicality of DNase as an effective therapeutic agent against biofilms.

Inspired by the mechanistic pathways and molecular structures of natural enzymes, chemists have recently put great effort into constructing a myriad of inexpensive enzyme mimics with high catalytic turnover and stability.[8] Synthetic biocatalysts based on Lewis acidic metal ions, such as Ce^{IV}, Zn^{II}, and Cu^{II}, have been widely studied as nuclease mimetics for accelerating the hydrolysis of DNA or RNA.[9] As a further evolution, multinuclear scaffolds such as metallomicelles, metallodendrimers, and monolayer-passivated gold nanoparticles (AuNPs), have been developed to confer cooperative catalytic effects, achieving higher hydrolytic activity.[10] In this sense, we envisioned that the construction of a versatile DNase mimic would provide unprecedented opportunities for anti-biofilm applications. Herein, we describe the design and synthesis of a robust and recoverable DNase-mimetic artificial enzyme (DMAE) and demonstrate its ability to prevent biofilm formation for prolonged periods of time, disperse established biofilms with good reusability, and eliminate biofilms when used in combination with traditional antibiotics.

[*] Z. Chen,[+] H. Ji,[+] C. Liu, W. Bing, Z. Wang, Prof. X. Qu
Laboratory of Chemical Biology and State Key Laboratory of Rare Earth Resources Utilization
Changchun Institute of Applied Chemistry
Chinese Academy of Sciences,
Changchun, Jilin 130022 (China)
E-mail: xqu@ciac.ac.cn
Z. Chen,[+] H. Ji,[+] C. Liu, W. Bing, Z. Wang
University of Chinese Academy of Sciences
Beijing 100039 (China)
Z. Chen[+]
Joint Department of Biomedical Engineering
University of North Carolina at Chapel Hill and North Carolina State University, Raleigh, NC 27695 (USA)
[+] These authors contributed equally to this work.

Supporting information for this article can be found under: http://dx.doi.org/10.1002/anie.201605296.

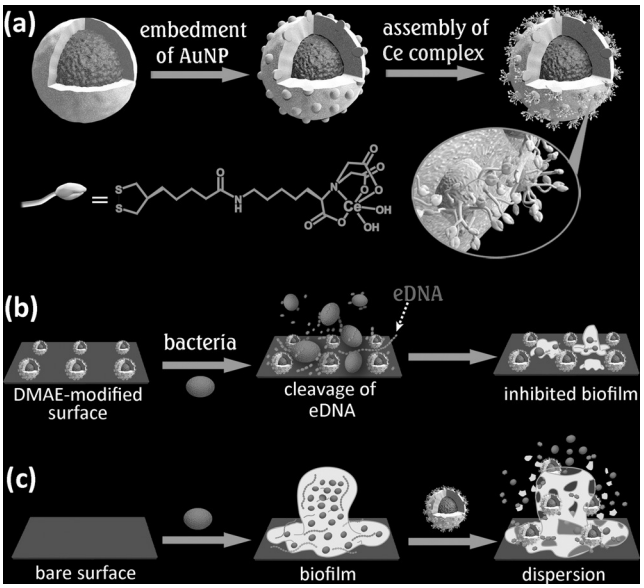

Scheme 1. Design of the DMAE for anti-biofilm applications. a) General procedure for the preparation of recoverable DMAEs by confining multiple multinuclear AuNPs covered with Ce complexes on the surface of Fe_3O_4/SiO_2 core/shell particles. b) Preventing bacterial adhesion and biofilm formation on DMAE-modified surfaces. c) Dispersion of preformed biofilms with subsequently added DMAE.

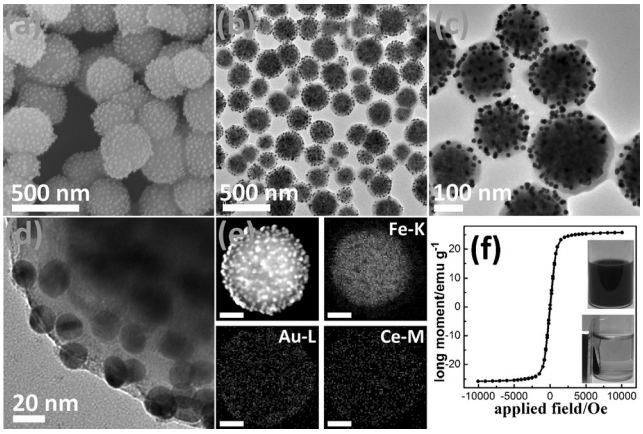

Figure 1. a) Scanning electron microscopy image (SEM), b) transmission electron microscopy image (TEM) image, and c, d) magnified TEM images of AuNPs confined on the surface of colloidal Fe_3O_4/SiO_2 core/shell particles. e) TEM elemental mappings of the Fe K edge, Au L edge, and Ce M edge signals in the synthesized DMAE; scale bars: 100 nm. f) Room-temperature magnetic hysteresis loop of DMAE; the inset shows photographs of a DMAE suspension (top) and the collection of DMAE in aqueous solution with a magnet (bottom).

As shown in Scheme 1 a, the DMAE was fabricated by physically confining AuNPs on the surface of colloidal magnetic Fe_3O_4/SiO_2 core/shell particles, which was followed by the assembly of one monolayer of Ce^{IV} nitrilotriacetic acid (NTA) complexes on the exposed AuNP surfaces to form the cooperative catalytic centers. Magnetic colloidal Fe_3O_4/SiO_2 core/shell particles were first obtained, and then the SiO_2 shell was modified with amino groups for subsequent absorption of citrate-capped AuNPs (16 nm; see the Supporting Information, Figures S1–S3). Afterwards, partial embedment of the AuNPs in a SiO_2 shell was achieved by another Stöber process (Figure 1 a–d and Figure S4), which selectively deposited an additional SiO_2 layer only on the preformed SiO_2 matrix but not on the Au surface owing to their differences in terms of surface chemistry.[11] As can be seen in Figure 1 d, within the second SiO_2 layer, more than half the volume of each AuNP had been embedded. Next, according to Schemes S1–S3, the partially exposed AuNP surface was covered with a monolayer of lipoic acid *N*-hydroxysuccinimide (Figure S5) through Au/S chemistry, and then (1*S*)-*N*-(5-amino-1-carboxypentyl)iminodiacetic acid (an NTA derivative; see Figures S6 and S7) was covalently conjugated to the activated ester for the coordination of Ce^{IV} to construct the final DMAE. The grafting of the ligand was confirmed by FTIR spectroscopy (Figure S8) while elemental mapping analysis showed the distribution of Fe, Au, and Ce in the DMAE particle (Figure 1 e). The amount of Ce^{IV} NTA complexes anchored on the DMAE particles was about 0.126 mmol g^{-1} as determined by elemental analysis and ICP-MS (Table S1). X-ray photon spectroscopy indicated that the cerium ions were in the +4 oxidation state (Figure S9). The paramagnetic properties of the DMAE (Figure 1 f) will facilitate its recovery with an external magnet and reusability.[12]

Next, the catalytic activity of DMAE in the hydrolysis of the DNA model substrate bis(4-nitrophenyl)phosphate (BNPP; Figures S10 and S11) and eDNA was investigated. Upon increasing the BNPP concentration at a fixed concentration of DMAE, a saturation profile was observed (Figure S11 c), indicating the binding of the substrate to the catalytic site prior to cleavage. The pseudo-first-order rate constant for BNPP cleavage was about $4.37\times10^{-5}\,s^{-1}$, and fitting of the data to the Michaelis–Menten equation yielded $1/K_M = 3300\,M^{-1}$ (Figure S11 d). The high affinity of the reactive site for the substrate supported the polynuclear nature of DMAE. Further inspection of the sigmoidal profile of the plot describing the initial rate versus the Ce^{4+}/NTA ratio confirmed the cooperativity of adjacent metal centers (Figure S12).[10e] Moreover, the catalytic activity of DMAE remained stable over at least six catalytic cycles (Figure S13). The activity of DMAE was higher than that of previously reported Ce^{IV} complexes but lower than that of Ce^{IV} hydroxides.[9] However, the latter suffer from very short activity and low stability.[9g] Afterwards, we explored the multivalency of DMAE towards the hydrolysis of natural DNAs. As the eDNA in biofilms is similar to the bacterial-genome DNA,[6g] the genomic DNA of *S. aureus* was extracted and used as the substrate. As can be seen from the agarose gel (1 %) electrophoresis (Figure 2 a), the DMAE effectively cleaved genomic DNA into smaller fragments with increasing incubation time. In contrast, control experiments using particles without Ce^{IV} (designed as $DMAE_{(no\ Ce)}$) or only buffer solution showed that the genomic DNA remained stable under these reaction conditions. These results confirm that the DNase-mimicking activity indeed originates from the multivalent Ce^{IV} centers. Moreover, the assembly of multiple functional ligands on each particle surface provided dense recognition units for interaction with DNA,[13] facilitating the cleavage reactions. Furthermore, DMAE exhibited good

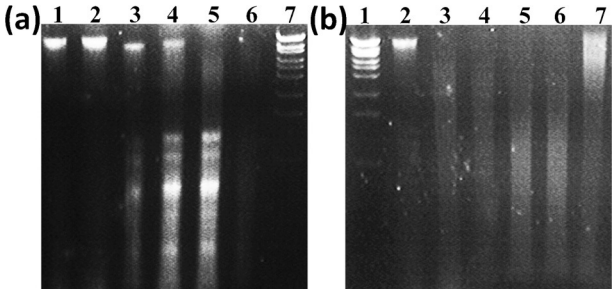

Figure 2. Cleavage of genomic DNA of *S. aureus* catalyzed by DMAE. a) Agarose gel (1%) electrophoresis showing DNA cleavage by DMAE for different incubation times. Lane 1: control with buffer only; lane 2: control with $DMAE_{(no\ Ce)}$; lanes 3–6: after 6, 12, 18, and 24 h, respectively; lane 7: DNA marker. b) Reusability of DMAE for the hydrolysis of genomic DNA. Lane 1: DNA marker; lane 2: untreated DNA; lanes 3–7: the first to fifth run.

reusability in cleaving DNAs over several cycles (Figure 2b). In contrast, no obvious degrading effect of DMAE was observed towards the other two main extracellular matrixes, polysaccharides (Figure S14) and proteins (Figure S15). Thus DMAE is expected to target eDNA when combating biofilms.

These encouraging results prompted us to evaluate the anti-biofilm potential of DMAE. To this end, we first examined its efficiency in inhibiting bacterial surface adhesion and biofilm formation (Scheme 1b). DMAE- and DNase I-coated surfaces were fabricated (Figures S16 and S17) and challenged with *S. aureus* suspensions. After 60 min incubation under static conditions, numerous *S. aureus* cells were attached to the bare and $DMAE_{(no\ Ce)}$-coated surfaces (Figure S18). The attachment of bacteria to the DMAE- and DNase I-coated surfaces was reduced by more than 92% and 95%, respectively, compared to the bare surface. Then, the biomass and average thickness of the biofilms formed on these surfaces were analyzed over time using crystal violet staining (Figure 3a,b) and 3D confocal microscopy (Figure 3c,d), respectively. Interestingly, significantly reduced adhesion (>90%) and much thinner biofilms (less than 5 μm) were observed for the DMAE-coated surfaces even after 120 h. However, for DNase I, the amount as well as the thickness of the adherent biofilm were low only up to 24 h of cultivation and increased gradually afterwards. Such differences could be attributed to the vulnerable nature of enzymes and the unique stability of synthetic biocatalysts, as the negligible antibacterial activity of both DMAE and DNase I excludes the possibility that the inhibition was caused by an effect on cell viability (Figure S19). In contrast, much thicker biofilms were formed on both control surfaces, which confirmed that the anti-biofilm activity of DMAE is due to the multinuclear metal centers.

To better understand the effects of DMAE on biofilm formation, the amount of eDNA present in each well of the above 24 h unwashed biofilms was measured by quantitative real-time PCR (qRT-PCR) using four different primer pairs specific for four randomly selected chromosomal genes (Table S2). As shown in Figure S20a, the average amount of eDNA present in the DNase I (4.58 ± 0.42 ng/well) and DMAE (7.24 ± 0.61 ng/well) groups was reduced by factors of about eight and five, respectively, compared with the bare surface group (36.27 ± 2.58 ng/well). In further experiments, we found that mixing purified genomic DNA with the suspensions from both the DNase I and DMAE groups could efficiently reverse the inhibition effect and accelerated the adherence of bacteria onto new bare surfaces to reform biofilms (Figure S20b). Biofilm formation has been described as a two-step process consisting of initial cell attachment to a surface and a subsequent accumulative phase, where eDNA is identified as a cell-to-substratum or cell-to-cell connecting component.[6] We therefore rationalized the suppressed bacterial adhesion and biofilm formation on DMAE-coated surfaces to be a result of efficient eDNA cleavage catalyzed

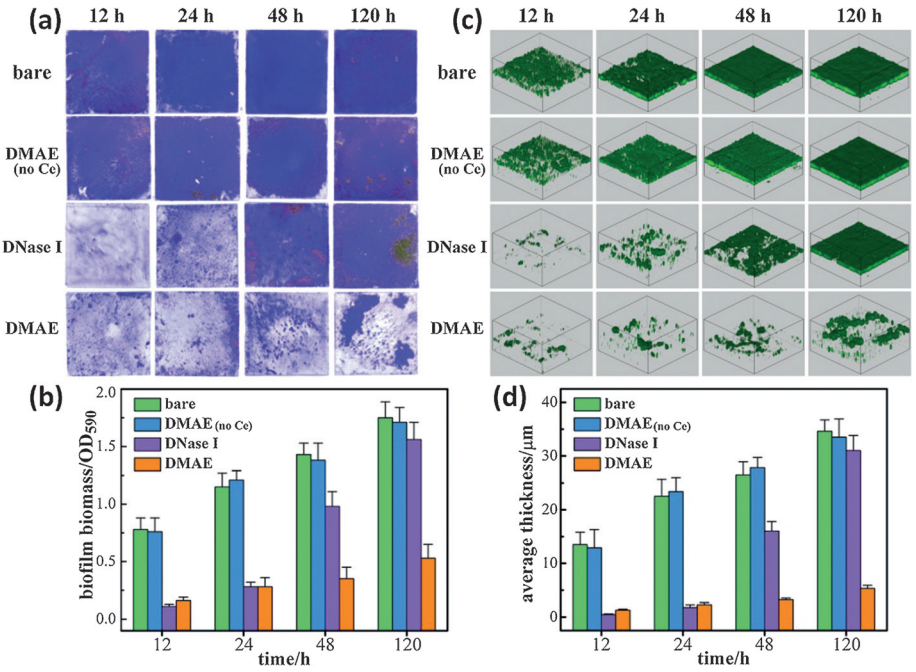

Figure 3. Inhibited biofilm formation on DMAE-modified surfaces. a) Biofilms formed on bare, $DMAE_{(no\ Ce)}$-, DNase I-, and DMAE-modified surfaces that were left to grow for different periods of time were stained with crystal violet. b) Quantitative analysis of the crystal-violet-stained biofilms in (a) by measuring the absorbance at $\lambda = 590$ nm; each bar represents the average of three experiments. c) 3D confocal laser scanning microscopy (CLSM) of biofilms formed on bare, $DMAE_{(no\ Ce)}$-, DNase I-, and DMAE-modified surfaces after different incubation times. Image sizes: 639.5 μm × 639.5 μm. The biofilms were stained with Calcein-AM. d) Average thickness of the biofilms shown in (c) as calculated by the COMASTAT software.[2b,c] Each bar was assessed using a minimum of five different images per plate from three independent experiments.

by the multinuclear DMAE. Overall, by taking advantage of the eDNA degradation ability and inherent stability of DMAE, prolonged inhibition of bacterial adhesion was achieved, which avoided the need of continuously adding fresh natural DNase to new generations of biofilms.

We next investigated whether DMAE could disperse established biofilms (Scheme 1 c). In this experiment, 24 h old *S. aureus* biofilms were treated with different concentrations of DMAE for 12 h. The remaining biomass and average thickness of the biofilms were markedly reduced by DMAE treatment in a dose-dependent manner (Figure S21). Furthermore, qRT-PCR experiments confirmed the reduction of the eDNA levels in the DMAE-treated wells (Figure S22). Structurally, eDNA is known to act as a "glue" that integrates bacteria and other EPS into sessile 3D frameworks.[6] The cleavage of eDNA by DMAE disrupted the interactions that kept all constituents together, which finally dispersed the biofilms. We further assessed the ability of DMAE towards dispersing biofilms of various ages. Unlike DNase I treatment, which only efficiently dissolved young biofilms ($\leq$ 24 hours old), the addition of DMAE caused significant biofilm detachment at all time points (Figure 4). Further experiments indicated that DNase I showed minimal penetration whereas DMAE effectively penetrated and diffused within the biofilms (Figure S23). This difference might be due to the effect of nanoparticle sedimentation, which increases the local concentration and uptake in biofilms, but sedimentation did not affect the DMAE nanoparticle size (Figure S24). Such an effect has been also observed in in vitro studies of eukaryotic cell–nanoparticle interactions.[13] Thus the resistance of more mature biofilms to DNase I could be attributed to the poor penetration of DNase I or the presence of proteolytic exoenzymes.[7] The age-independent dispersion capability of DMAE might be due to its efficient penetration, natural stability, and multivalent interactions with eDNA in EPS.[14] Therefore, it can be deduced that DMAE is better adapted to disrupt the eDNA present in biofilms.

We also studied the reusability of DMAE as it can be easily recovered with the help of an external magnet. As can be seen in Figure S25, the attached biofilm remained thin even after five rounds of reusing DMAE whereas natural DNases have hardly been reused thus far. The good reusability of DMAE could be ascribed to its stability under harsh conditions, as confirmed by ICP-MS; less than 10 % of the metal centers had been lost after five cycles of dispersing biofilms (Figure S26). Therefore, these attractive features make DMAE a more viable agent for dispersing preformed biofilms than DNase I in terms of operational stability and reusability. Although DMAE clearly cleaves DNA and exhibits anti-biofilm activity, we cannot exclude the possibility that DMAE also interferes with other factors (e.g., nonspecific adsorption induced inhibition of important exoenzymes)[1a] that may contribute to biofilm formation and integrity, and further studies are still required to address this point.

Finally, we tested the effect of DMAE on biofilms when used in combination with traditional antibiotics (Figure S27). In the presence of DMAE, ampicillin, levofloxacin, and rifampin led to a further decrease in the CFU (number of colony-forming units)/well values by 2.5, 1.8, and 2.1 log units, respectively, compared to control biofilms that were treated with equivalent antibiotics alone. Biofilms are notoriously resistant to antibiotics because EPS provides a strong and enduring support structure that protects the cells by inactivating or limiting the diffusion of antibiotics.[3,5,6g] Our data thus suggest that destructing the integrity of EPS by DMAE increases the availability of antibiotics to the cells, and as a result, the antibiotics are more effective in reducing the number of CFUs. Hence, the synergetic effect of DMAE and existing antibiotics offers a new strategy to overcome the tolerance of biofilms and finally eradicate the biofilms.

In summary, we have successfully constructed a multifunctional DNA-cleavage artificial enzyme. We have demonstrated that it inhibits biofilm formation for prolonged periods of time and eliminates biofilms in the presence of antibiotics. With multiple multinuclear-metal-complex protected AuNPs confined on each colloidal magnetic Fe_3O_4/SiO_2 core/shell particle, the synthetic biocatalyst exhibited high activity towards the cleavage of both model substrates and natural DNA. By degrading the eDNA present in the EPS, the DMAE not only strongly reduced bacterial adhesion and prevented biofilm formation over 120 h, but also effectively dispersed preformed biofilms of varying ages and could be magnetically recovered and recycled for five runs. Moreover, disrupting the integrity of EPS by DMAE greatly increased the activity of antibiotics towards killing the enclosed bacteria, finally eliminating the biofilms. Notably, from a wider perspective, these unique properties of DMAE offer promising features towards the design and construction of alternative types of EPS-degrading artificial enzymes for anti-biofilm applications.

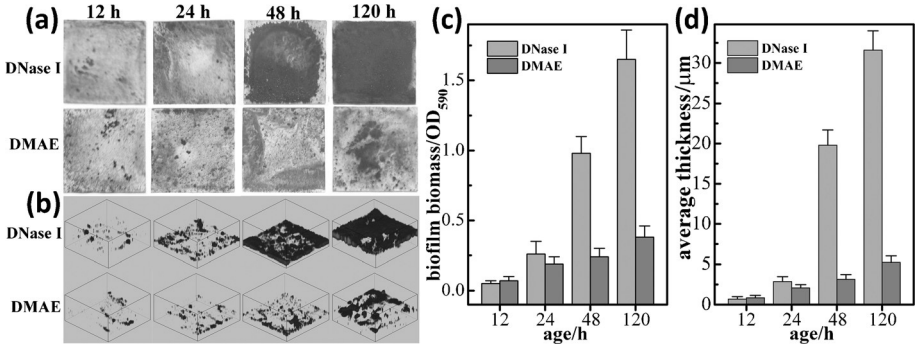

Figure 4. The effect of DMAE on established biofilms. a, c) Crystal violet staining and b, d) 3D CLSM imaging of biofilms of different ages after treatment with DMAE and DNase I. The biomass was determined by measuring the absorbance at $\lambda = 590$ nm. The size of each CLSM image is 639.5 μm × 639.5 μm, and the average thickness was calculated by using the COMASTAT software. Each bar represents the average of three experiments.

Acknowledgements

Financial support was provided by the National Basic Research Program of China (2012CB720602 and 2011CB936004) and the National Natural Science Foundation of China (21210002, 21431007, and 21533008).

Keywords: artificial enzymes · bacteria · biofilms · DNase · extracellular DNA

How to cite: *Angew. Chem. Int. Ed.* **2016**, *55*, 10732–10736
Angew. Chem. **2016**, *128*, 10890–10894

[1] a) H.-C. Flemming, J. Wingender, *Nat. Rev. Microbiol.* **2010**, *8*, 623; b) V. Berk, J. C. N. Fong, G. T. Dempsey, O. N. Develioglu, X. Zhuang, J. Liphardt, F. H. Yildiz, S. Chu, *Science* **2012**, *337*, 236.

[2] a) T.-F. Mah, B. Pitts, B. Pellock, G. C. Walker, P. S. Stewart, G. A. O'Toole, *Nature* **2003**, *426*, 306; b) A. Heydorn, B. K. Ersbøll, M. Hentzer, M. R. Parsek, M. Givskov, S. Molin, *Microbiology* **2000**, *146*, 2409; c) A. Heydorn, A. T. Nielsen, M. Hentzer, C. Sternberg, M. Givskov, B. K. Ersboll, S. Molin, *Microbiology* **2000**, *146*, 2395; d) N. G. Durmus, E. N. Taylor, K. M. Kummer, T. J. Webster, *Adv. Mater.* **2013**, *25*, 5706–5713; e) M. Eshed, J. Lellouche, A. Gedanken, E. Banin, *Adv. Funct. Mater.* **2014**, *24*, 1382.

[3] a) G. G. Anderson, J. J. Palermo, J. D. Schilling, R. Roth, J. Heuser, S. J. Hultgren, *Science* **2003**, *301*, 105; b) B. Duncan, X. Li, R. F. Landis, S. T. Kim, A. Gupta, L.-S. Wang, R. Ramanathan, R. Tang, J. A. Boerth, V. M. Rotello, *ACS Nano* **2015**, *9*, 7775; c) T.-K. Nguyen, R. Selvanayagam, K. K. K. Ho, R. Chen, S. K. Kutty, S. A. Rice, N. Kumar, N. Barraud, H. T. T. Duong, C. Boyer, *Chem. Sci.* **2016**, *7*, 1016; d) W. Bing, Z. Chen, H. Sun, P. Shi, N. Gao, J. Ren, X. Qu, *Nano Res.* **2015**, *8*, 1648.

[4] a) H. T. T. Duong, K. Jung, S. K. Kutty, S. Agustina, N. N. M. Adnan, J. S. Basuki, N. Kumar, T. P. Davis, N. Barraud, C. Boyer, *Biomacromolecules* **2014**, *15*, 2583; b) T. Mattila-Sandholm, G. Wirtanen, *Food Rev. Int.* **1992**, *8*, 573; c) F. Natalio, R. Andre, A. F. Hartog, B. Stoll, K. P. Jochum, R. Wever, W. Tremel, *Nat. Nanotechnol.* **2012**, *7*, 530.

[5] a) D. Schultz, J. N. Onuchic, E. Ben-Jacob, *Proc. Natl. Acad. Sci. USA* **2012**, *109*, 18633; b) I. Kolodkin-Gal, D. Romero, S. Cao, J. Clardy, R. Kolter, R. Losick, *Science* **2010**, *328*, 627; c) T. Böttcher, I. Kolodkin-Gal, R. Kolter, R. Losick, J. Clardy, *J. Am. Chem. Soc.* **2013**, *135*, 2927; d) W. Wei, W. Bing, J. Ren, X. Qu, *Chem. Commun.* **2015**, *51*, 12677; e) Y. Zhao, Z. Chen, Y. Chen, J. Xu, J. Li, X. Jiang, *J. Am. Chem. Soc.* **2013**, *135*, 12940; f) A. T. Garrison, Y. Abouelhassan, D. Kallifidas, F. Bai, M. Ukhanova, V. Mai, S. Jin, H. Luesch, R. W. Huigens, *Angew. Chem. Int. Ed.* **2015**, *54*, 14819; *Angew. Chem.* **2015**, *127*, 15032; N. Barraud, B. G. Kardak, N. R. Yepuri, R. P. Howlin, J. S. Webb, S. N. Faust, S. Kjelleberg, S. A. Rice, M. J. Kelso, *Angew. Chem. Int. Ed.* **2012**, *51*, 9057; *Angew. Chem.* **2012**, *124*, 9191.

[6] a) T. Das, B. P. Krom, H. C. van der Mei, H. J. Busscher, P. K. Sharma, *Soft Matter* **2011**, *7*, 2927; b) M. J. Huseby, A. C. Kruse, J. Digre, P. L. Kohler, J. A. Vocke, E. E. Mann, K. W. Bayles, G. A. Bohach, P. M. Schlievert, D. H. Ohlendorf, C. A. Earhart, *Proc. Natl. Acad. Sci. USA* **2010**, *107*, 14407; c) Z. Qin, Y. Ou, L. Yang, Y. Zhu, T. Tolker-Nielsen, S. Molin, D. Qu, *Microbiology* **2007**, *153*, 2083; d) T. Das, P. K. Sharma, H. J. Busscher, H. C. van der Mei, B. P. Krom, *Appl. Environ. Microbiol.* **2010**, *76*, 3405; e) L. K. Jennings, K. M. Storek, H. E. Ledvina, C. Coulon, L. S. Marmont, I. Sadovskaya, P. R. Secor, B. S. Tseng, M. Scian, A. Filloux, D. J. Wozniak, P. L. Howell, M. R. Parsek, *Proc. Natl. Acad. Sci. USA* **2015**, *112*, 11353; f) E. E. Mann, K. C. Rice, B. R. Boles, J. L. Endres, D. Ranjit, L. Chandramohan, L. H. Tsang, M. S. Smeltzer, A. R. Horswill, K. W. Bayles, *PLoS ONE* **2009**, *4*, e5822; g) M. Lappann, H. Claus, T. Van Alen, M. Harmsen, J. Elias, S. Molin, U. Vogel, *Mol. Microbiol.* **2010**, *75*, 1355; h) H.-H. Liu, Y.-R. Yang, X.-C. Shen, Z.-L. Zhang, P. Shen, Z.-X. Xie, *Curr. Microbiol.* **2008**, *57*, 139.

[7] a) J. J. T. M. Swartjes, T. Das, S. Sharifi, G. Subbiahdoss, P. K. Sharma, B. P. Krom, H. J. Busscher, H. C. van der Mei, *Adv. Funct. Mater.* **2013**, *23*, 2843; b) C. B. Whitchurch, T. Tolker-Nielsen, P. C. Ragas, J. S. Mattick, *Science* **2002**, *295*, 1487; c) R. Nijland, M. J. Hall, J. G. Burgess, *PLoS ONE* **2010**, *5*, e15668; d) G. V. Tetz, N. K. Artemenko, V. V. Tetz, *Antimicrob. Agents Chemother.* **2009**, *53*, 1204; e) E. A. Izano, M. A. Amarante, W. B. Kher, J. B. Kaplan, *Appl. Environ. Microbiol.* **2008**, *74*, 470.

[8] a) G. Y. Tonga, Y. Jeong, B. Duncan, T. Mizuhara, R. Mout, R. Das, S. T. Kim, Y.-C. Yeh, B. Yan, S. Hou, V. M. Rotello, *Nat. Chem.* **2015**, *7*, 597; b) Y. Lin, J. Ren, X. Qu, *Acc. Chem. Res.* **2014**, *47*, 1097; c) H. Sun, N. Gao, K. Dong, J. Ren, X. Qu, *ACS Nano* **2014**, *8*, 6202; d) Z. Chen, C. Zhao, E. Ju, H. Ji, J. Ren, B. P. Binks, X. Qu, *Adv. Mater.* **2016**, *28*, 1682; e) Y. Song, K. Qu, C. Zhao, J. Ren, X. Qu, *Adv. Mater.* **2010**, *22*, 2206; f) A. A. Vernekar, D. Sinha, S. Srivastava, P. U. Paramasivam, P. D'Silva, G. Mugesh, *Nat. Commun.* **2014**, *5*, 5301; g) K. Li, K. Wang, W. Qin, S. Deng, D. Li, J. Shi, Q. Huang, C. Fan, *J. Am. Chem. Soc.* **2015**, *137*, 4292; h) B. Liu, Z. Sun, P.-J. J. Huang, J. Liu, *J. Am. Chem. Soc.* **2015**, *137*, 1290–1295; i) C. Zhang, W. Bu, D. Ni, S. Zhang, Q. Li, Z. Yao, J. Zhang, H. Yao, Z. Wang, J. Shi, *Angew. Chem. Int. Ed.* **2016**, *55*, 2101; *Angew. Chem.* **2016**, *128*, 2141.

[9] a) M. Livieri, F. Mancin, G. Saielli, J. Chin, U. Tonellato, *Chem. Eur. J.* **2007**, *13*, 2246; b) M. E. Branum, A. K. Tipton, S. Zhu, L. Que, *J. Am. Chem. Soc.* **2001**, *123*, 1898; c) Y. Jin, J. A. Cowan, *J. Am. Chem. Soc.* **2005**, *127*, 8408; d) A. A. Neverov, C. T. Liu, S. E. Bunn, D. Edwards, C. J. White, S. A. Melnychuk, R. S. Brown, *J. Am. Chem. Soc.* **2008**, *130*, 6639; e) Y. Xu, Y. Suzuki, T. Lönnberg, M. Komiyama, *J. Am. Chem. Soc.* **2009**, *131*, 2871; f) A. L. Maldonado, A. K. Yatsimirsky, *Org. Biomol. Chem.* **2005**, *3*, 2859; g) J. Sumaoka, Y. Azuma, M. Komiyama, *Chem. Eur. J.* **1998**, *4*, 205.

[10] a) R. Bonomi, F. Selvestrel, V. Lombardo, C. Sissi, S. Polizzi, F. Mancin, U. Tonellato, P. Scrimin, *J. Am. Chem. Soc.* **2008**, *130*, 15744; b) M. Diez-Castellnou, F. Mancin, P. Scrimin, *J. Am. Chem. Soc.* **2014**, *136*, 1158; c) B. Gruber, E. Kataev, J. Aschenbrenner, S. Stadlbauer, B. König, *J. Am. Chem. Soc.* **2011**, *133*, 20704; d) M. Martin, F. Manea, R. Fiammengo, L. J. Prins, L. Pasquato, P. Scrimin, *J. Am. Chem. Soc.* **2007**, *129*, 6982; e) R. Bonomi, P. Scrimin, F. Mancin, *Org. Biomol. Chem.* **2010**, *8*, 2622; f) C. Pezzato, P. Scrimin, L. J. Prins, *Angew. Chem. Int. Ed.* **2014**, *53*, 2104; *Angew. Chem.* **2014**, *126*, 2136.

[11] Y. Hu, Y. Sun, *J. Am. Chem. Soc.* **2013**, *135*, 2213.

[12] a) D.-H. Kim, E. A. Rozhkova, I. V. Ulasov, S. D. Bader, T. Rajh, M. S. Lesniak, V. Novosad, *Nat. Mater.* **2010**, *9*, 165–171; b) E. A. Vitol, V. Novosad, E. A. Rozhkova, *Nanomedicine* **2012**, *7*, 1611.

[13] E. C. Cho, Q. Zhang, Y. Xia, *Nat. Nanotechnol.* **2011**, *6*, 385.

[14] L.-S. Wang, A. Gupta, V. M. Rotello, *ACS Infect. Dis.* **2016**, *2*, 3.

Received: May 31, 2016
Revised: July 4, 2016
Published online: August 2, 2016

